Journal of Alloys and Compounds 509 (2011) 105–113

Contents lists available at ScienceDirect

Journal of Alloys and Compounds

journal homepage: www.elsevier.com/locate/jallcom

The effects of thermal treatment on the physical properties of $Sr_2FeMo_{1-x}M_xO_6$ perovskite with M = W, Ta and $x \leq 0.3$

E. Burzo[a,*], I. Balasz[a], M. Valeanu[b], I.G. Pop[c]

[a] Faculty of Physics, Babes Bolyai University, 400084 Cluj-Napoca, Romania
[b] National Institute of Material Physics, PO Box MG-07, Bucharest, Romania
[c] Emmanuel University, Oradea, Romania

ARTICLE INFO

Article history:
Received 18 June 2010
Received in revised form 12 August 2010
Accepted 25 August 2010

Keywords:
Perovskite
Crystal structure
Magnetic moments
Magnetoresistivity

ABSTRACT

The $Sr_2FeMo_{1-x}M_xO_6$ double perovskites with M = W and Ta and $x \leq 0.3$, were obtained by sintering at 1300 °C, during 4 and 8 h, respectively. The perovskites crystallize in a tetragonal structure having *I4/mmm* space group. The grains are more homogeneous when sintering time is increased. The samples sintered longer time show higher values of saturation magnetizations, resistivities and magnetoresistivities than the samples sintered during 4 h. The intergrain tunnelling magnetoresistance as well as the intragrain contributions, respectively were analysed as function of temperature and external field. The changes in the physical properties, when the sintering time is increased, have been correlated with the number of antisite defects as well as the nature of grain boundaries.

1. Introduction

In the ordered perovskite $A_2B'B''O_6$, where A is an alkaline-earth, the transition-metal sites are occupied alternatively by cations B′ and B″. A complete ordering can be shown if the charge difference between B′ and B″ ions is grater than 2 [1]. The actual degree of ordering depends mainly on the synthesis conditions and is primarily controlled by kinetic processes. As a rule, increasing order may be obtained with increasing synthesis temperature or treatment times.

The Sr_2FeMoO_6 perovskite exhibits intrinsic tunnelling-type magnetoresistance, at room temperature [2]. The origin of this behaviour was explained starting from electronic structure calculations that indicated the material to be half metallic. The down-spin conduction band crossing the Fermi level, E_F, is dominated by Fe3d–Mo4d t_{2g} states while the up-spin band, below E_F, is mostly due to Fe3d e_g ones [2]. The resistance of the sample is dominated by the charge carrier scattering at the grain boundaries. The temperature dependence of the low field magnetoresistance was shown to follow the same trend as that of the square of reduced magnetization [2]. The resistivity values depend critically on the sample preparation procedure. The half-metallic behaviour has been reached under the assumption of a perfect ordered crystalline structure. The spin polarization, *P*, for Sr_2FeMoO_6 single crystals with 11–16% of B-site disorder was measured [3]. The highest polarization value was *P* = 70%. The computed value *P* = 53%, for a degree of B-site disorder of 12.5%, was in good agreement with experimental data.

The antisite disorder in Sr_2FeMoO_6, of the Mo atoms at the Fe position and vice versa, influences their magnetic and magnetotransport properties. A neutron diffraction study was performed on two polycrystalline Sr_2FeMoO_6 samples showing ≅70% and ≅18%, respectively, cationic ordering [4]. The data, on a most disordered Sr_2FeMoO_6 sample, supported the hypothesis that near-neighbour Fe–Fe atoms are antiferromagnetically (AFM) coupled by virtue of strong superexchange Fe–O–Fe interactions. The coherence of the AFM arrangement of neighbouring Fe–O–Fe regions was maintained across the crystal by AFM Fe–O–Mo superexchange interactions. Magnetic moments of 3.9(1) μ_B, and −0.37(6) μ_B, at the Fe and Mo positions, respectively were shown in sample having 70% cation order [4].

The iron valence states in the Sr_2FeMoO_6 have been studied. There were no agreement between the reported data. The iron valence states, from those close to Fe^{2+} [5] to those involving also an amount of Fe^{3+} [6–9], up to 50% Fe^{2+}–50% Fe^{3+} [9–11], were reported. As example, in highly ordered Sr_2FeMoO_6 has been shown iron mixed valence states 30% Fe^{3+}–Mo^{5+} and 70% Fe^{2+}–Mo^{6+} [10]. One possible reason for these discrepancies may be complex intra- and intergrain structure on Sr_2FeMoO_6 interfaces [12,13]. It has been shown also that Sr_2FeMoO_6 decomposes gradually with time into $SrMoO_4$, leading to a structural transformation of the system [14]. Kuepper et al. [15] reported a

* Corresponding author. Tel.: +40 264 405300; fax: +40 264 591906.
E-mail address: burzo@phys.ubbcluj.ro (E. Burzo).

0925-8388/$ – see front matter © 2010 Elsevier B.V. All rights reserved.
doi:10.1016/j.jallcom.2010.08.126

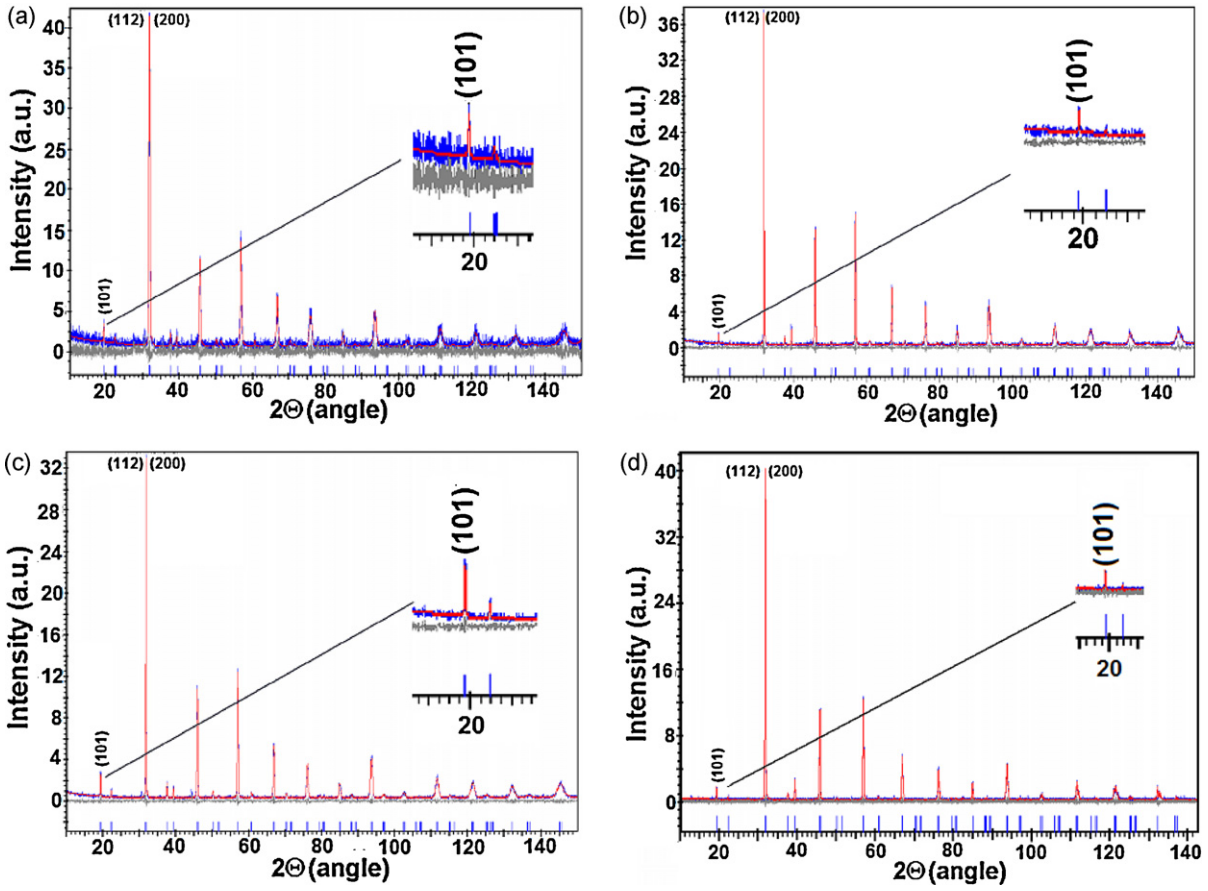

Fig. 1. XRD patterns of $Sr_2FeMo_{0.7}M_{0.3}O_6$ with M = W (a and b) and Ta (c and d) sintered at 1300 °C, during 4 h (a and c) and 8 h (b and d), respectively.

mixed valence Fe^{2+}, Fe^{3+} state, which shifts toward Fe^{3+} with time.

The Sr_2FeWO_6 is an antiferromagnetic insulator having localized high-spin configuration at the Fe^{2+} ions [16,17]. The $Sr_2FeMo_{1-x}W_xO_6$ solid solutions were studied [9,17–24]. Structural characterization showed an overall volume cell expansion upon W substitution, accompanied by a smooth evolution of lattice parameters. As the W content exceeds $x = 0.75$, a metal-insulator (MIT) transition occurs [22]. For a similar elaborated series, the W doping, generally allows the enhancement of the chemical order [20,21,23].

The Sr_2FeTaO_6 is a double perovskite having cubic-type structure with no ordering of cations on the transition-metal sublattice [24–26]. The perovskite shows a spin-glass behaviour [26]. The presence of $Sr_2FeMo_{1-x}Ta_xO_6$ solid solutions has been shown in all the composition range [24,27]. Ta substitution has a stronger influence on the transport properties and magnetization than W substitution has. It was suggested that Ta^{5+} disrupts the double exchange interactions, responsible for the magnetism in the Sr_2FeMoO_6, more efficiently than W^{6+}. A Mössbauer effect study performed on $Sr_2FeMo_{1-x}M_xO_6$ with M = W, Ta showed that W^{6+} substitution causes increasing amount of Fe to enter Fe^{2+}, whereas Ta^{5+} substitution yields increasing amount of Fe^{3+} [27]. Both substitutions lead a decrease in intensity of the component assigned to $Fe^{2.5+}$, which for $x = 0.3$ is of 70%. In both solid solution systems, the mean charge difference between B and B′ cations is generally higher than two, particularly for low doping content.

In the following we analyse the effect of thermal treatment on the magnetic properties and magnetoresistivities of $Sr_2FeMo_{1-x}W_xO_6$ solid solutions with $x \leq 0.3$, thermally treated at 1300 °C during 4 and 8 h, respectively. In addition, some structural and magnetic data on $SrFeMo_{0.7}Ta_{0.3}O_6$, obtained by similar procedure as that of the W-substituted double perovskites, will be given.

2. Experimental

The $Sr_2FeMo_{1-x}M_xO_6$ double perovskites with M = W or Ta and $x \leq 0.3$, were prepared by solid state reaction. The stoichiometric quantities of $SrCO_3$, Fe_2O_3, MoO_3, WO_3 and Ta_2O_5 powders were mixed and calcinated, in argon atmosphere, at 900 °C. The calcinated powders were pelletized and sintered at 1300 °C, during 4 h and 8 h, respectively, in argon having 3% hydrogen.

The phase purity, crystal structure and lattice parameters were investigated by X-ray diffraction, in Bragg–Brentano geometry, by using a Seifert-type equipment and CuK_α radiation ($\lambda = 1.54059$ Å). The data were collected in steps of $2\theta = 0.04°$ over the range $10° \leq 2\theta \leq 148°$. The spectra were analysed by Rietveld method by using the TOPAS program [28,29]. The positions of the atoms and lattice parameters were determined.

Scanning electron microscopy (SEM) and energy disperse spectroscopy (EDS) measurements were made using a JEOL-type equipment on polished samples. The grain dimensions and the distribution of constituting elements inside the grains were analysed. The composition of the grains was also determined, in a depth from surface up to 200 Å.

Magnetic measurements have been performed by extraction method in the temperature range 4 K to the Curie points, T_c, in fields up to 7 T. The resistivities and magnetoresistivities were studied between 10 K and 300 K in fields up to 7 T, by using the four terminal methods.

3. Experimental results

3.1. Structural properties

The studied compounds crystallize in the tetragonal structure having space group *I*4/*mmm*. As example, the XRD spectra of the $Sr_2FeMo_{0.7}W_{0.3}O_6$ and $Sr_2FeMo_{0.7}Ta_{0.3}O_6$ perovskites sintered at 1300 °C, during 4 and 8 h, respectively are given in Fig. 1. The XRD

Table 1
Crystallographic properties and the positions of O1 and O2 oxygens in lattice, as well as of the number of antisites.

Sample	Lattice constants (Å)		$O1_{x,y}$[a]	$O2_z$[a]	$I(1\,0\,1)$	Volume (Å^3)	Gof[b]
	a	c			$I(2\,0\,0)+I(1\,1\,2)$		
$Sr_2FeMo_{0.7}W_{0.3}O_6$ (4 h)	5.5784(1)	7.9266(5)	0.24576	0.24576	12.8	246.7	1.22
$Sr_2FeMo_{0.7}W_{0.3}O_6$ (8 h)	5.5887(2)	7.9127(7)	0.24672	0.24672	10.5	247.1	1.51
$Sr_2FeMo_{0.9}W_{0.1}O_6$ (4 h)	5.583(4)	7.9110(6)	0.25273	0.25273	22.5	246.6	1.23
$Sr_2FeMo_{0.9}W_{0.1}O_6$ (8 h)	5.5821(4)	7.9085(5)	0.25375	0.25375	19.5	246.4	1.33
$Sr_2FeMo_{0.7}Ta_{0.3}O_6$ (4 h)	5.5861(3)	7.9172(6)	0.27107	0.27107	2.94	247.1	1.54
$Sr_2FeMo_{0.7}Ta_{0.3}O_6$ (8 h)	5.5858(6)	7.9140(9)	0.27591	0.27591	2.10	246.9	1.46
Sr_2FeMoO_6	5.573(5)	7.902(1)	0.2536	0.2536	3.0	245.47	1.09

[a] The $O1_z = O2_x = O2_y = 0$ positions were fixed for all compositions and sintering time.
[b] The goodness-of-fit (Gof) is given by the ratio of weighted profile factor (R_{wp}) and expected weighted profile factor R_{exp}, Gof = R_{wp}/R_{exp}.

lines are narrower in the case of samples sintered during 8 h. The lattice constants increase, when W and Ta content is higher, particularly the c parameters. The above behaviour can be correlated with a greater radius of W^{6+}(0.60 Å) and Ta^{6+} (0.64 Å) ions, as compared to those of Mo^{6+} (0.59 Å) or Mo^{5+} (0.61 Å) ones. The presence of mixed valence states Fe^{2+}–Mo^{6+} and Fe^{3+}–Mo^{5+} influences also in some extend the lattice constants. The axial ratio $c/a\sqrt{2}$ is higher in samples sintered 4 h. Values 1.0049 and 1.0023 were obtained for $x = 0.3$ and M = W and Ta, respectively. In case of the samples sintered 8 h, the axial ratio decreases from a value 1.0028 ($x = 0$) to 1.0019 ($x = 0.1$) and 1.0013 ($x = 0.3$) in $Sr_2FeMo_{1-x}W_xO_6$ system and up to 1.0019 in $Sr_2FeMo_{0.7}Ta_{0.3}O_6$. The volumes of the cells, for a given composition, are generally decreasing, when the sintering time is longer. This fact can be interpreted by improving the

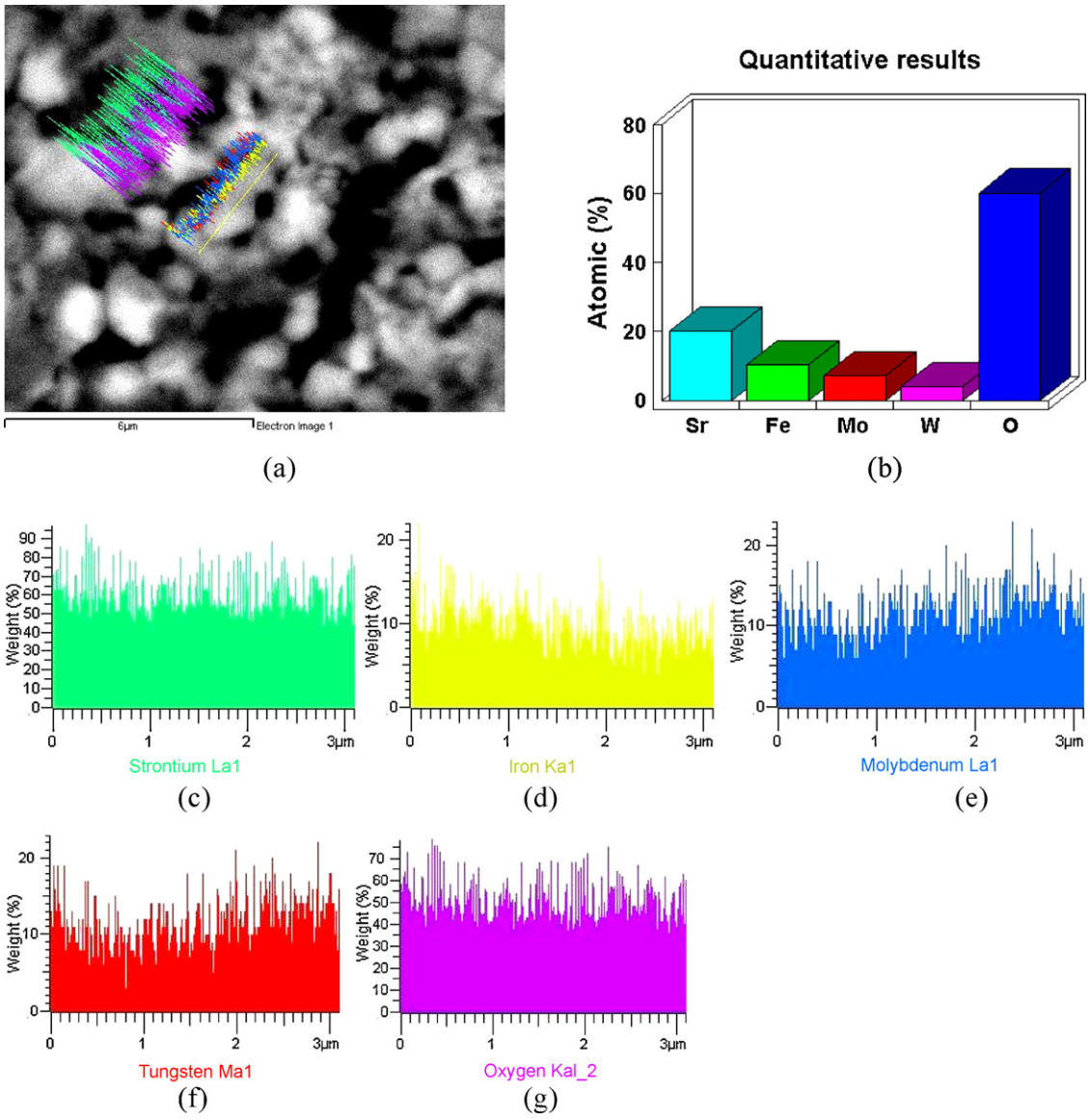

Fig. 2. SEM pattern (a), grain composition (b) and distribution of constituting elements along a line scan (c–g) for W doped sample with $x = 0.3$, sintered 4 h. The grain composition is $Sr_2Fe_{1.01}Mo_{0.67}W_{0.26}O_{5.92}$.

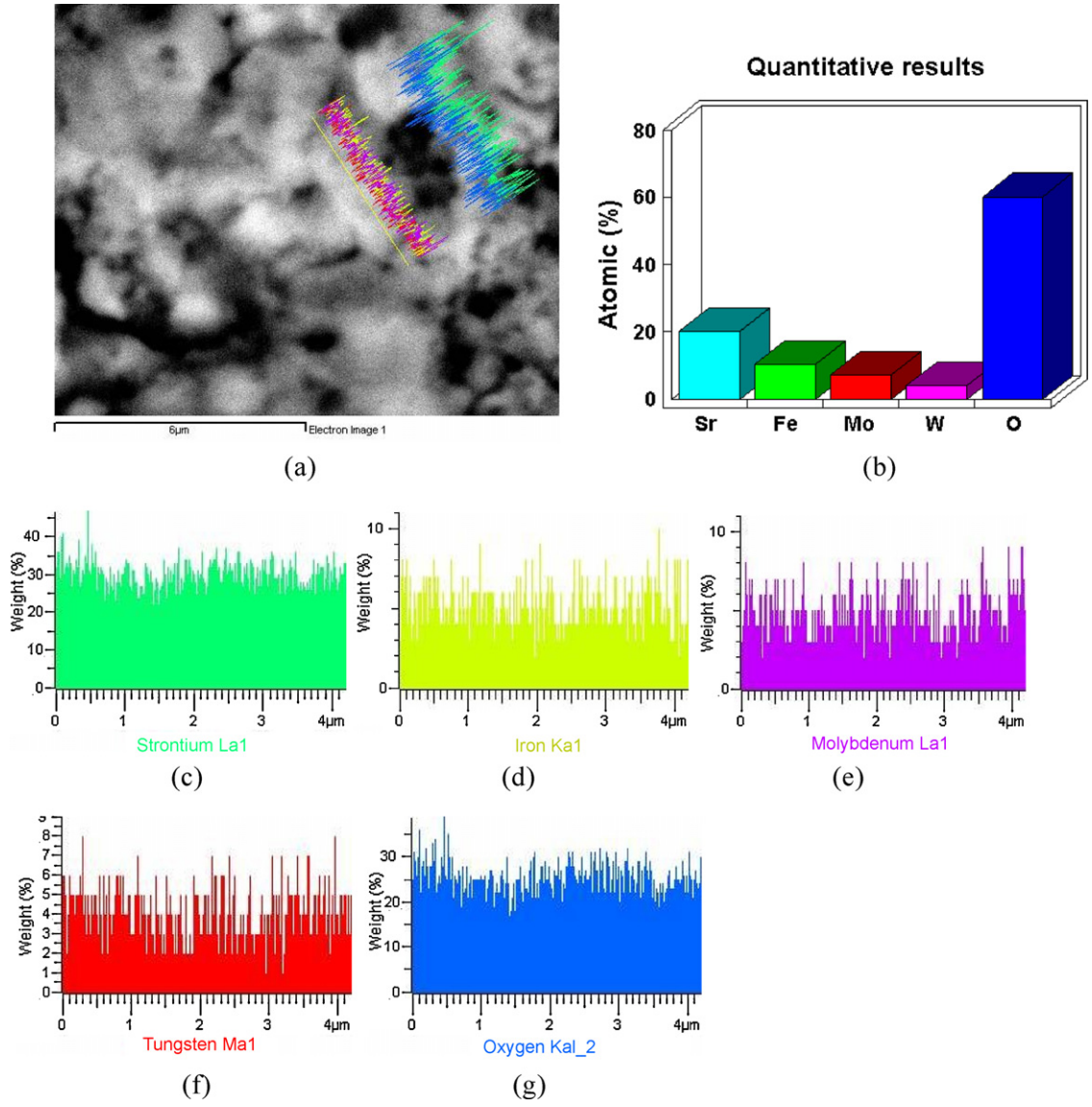

Fig. 3. SEM pattern (a), grain composition (b) and distribution of constituting elements along a line scan (c–g) for a W doped sample with $x = 0.3$ sintered 8 h. The grain composition is $Sr_2Fe_{1.02}Mo_{0.72}W_{0.33}O_{6.03}$.

cation ordering, decreasing the number of antisites, respectively. This is in agreement with the antisite content determined from the intensities of the (1 0 1), (2 0 0) and (1 1 2) lines of XRD spectra, as $I(1\,0\,1)/[I(2\,0\,0)+I(1\,1\,2)]$. In a well crystallized Sr_2FeMoO_6, the number of antisites, obtained from the above relation was ≅3% [10]. In $Sr_2FeMo_{0.7}W_{0.3}O_6$, the number of antisites decreased from 12.8% to 10.5%, when increasing the annealing time from 4 to 8 h. High antisite content has been shown in $Sr_2FeMo_{0.9}W_{0.1}O_6$ sintered 4 and 8 h, respectively although the same procedure of preparation has been used as for $x = 0.3$ sample (Table 1). A rather small number of antisites have been shown also by sintering of $Sr_2FeMo_{0.7}Ta_{0.3}O_6$ samples, at 1300 °C. This is not expected since the difference in the mean charge of B and B′ cations is smaller than in the case of W-substituted samples, although higher than 2. Probably that the high sintering temperature, of 1300 °C, can be one of the reasons. The commonly sintering temperature reported for this system was 1150 °C [24,27]. This matter is interesting and will be further analysed.

The SEM and EDS studies were performed on 4–6 samples for each composition and sintering time, in order to obtain information of the grain dimensions and their compositions. As example, in Figs. 2 and 3 are presented the SEM patterns, as well as the grain compositions for $Sr_2FeMo_{0.7}W_{0.3}O_6$ samples sintered at 1300 °C, 4 and 8 h, respectively. In the case of samples sintered at 4 h, the forms of the grains are rather irregular, having dimensions between 1 and 2 μm. The dimensions of the grains in samples sintered during 8 h, increased at 2–3 μm and their forms are more regular.

The EDS analyses showed some differences in the compositions of the grains for the same sample. The content of constituting elements was normalized to two Sr atoms. In the case of sample with initial $x = 0.3$ W content, sintered during 4 h, the compositions of the grains covered the ranges $Sr_2Fe_{0.96-1.01}Mo_{0.67-0.78}W_{0.26-0.33}O_{5.92-6.05}$, with a mean composition of the six grains as $Sr_2Fe_{0.988}Mo_{0.697}W_{0.308}O_{6.03}$. By sintering during 8 h, there was a more narrow difference between the grain compositions, namely $Sr_2Fe_{0.98-1.02}Mo_{0.69-0.72}W_{0.29-0.33}O_{5.94-6.04}$, with a mean content of $Sr_2FeMo_{0.71}W_{0.32}O_{6.01}$. The same behaviour was shown for the samples with $x = 0.1$ W. The smaller differences in the composition for the grains in samples sintered longer time are in agreement with their narrower XRD lines, as shown in Fig. 1. We conclude that a more uniform composition of the grains can be obtained by increasing sintering time. We note that the errors in

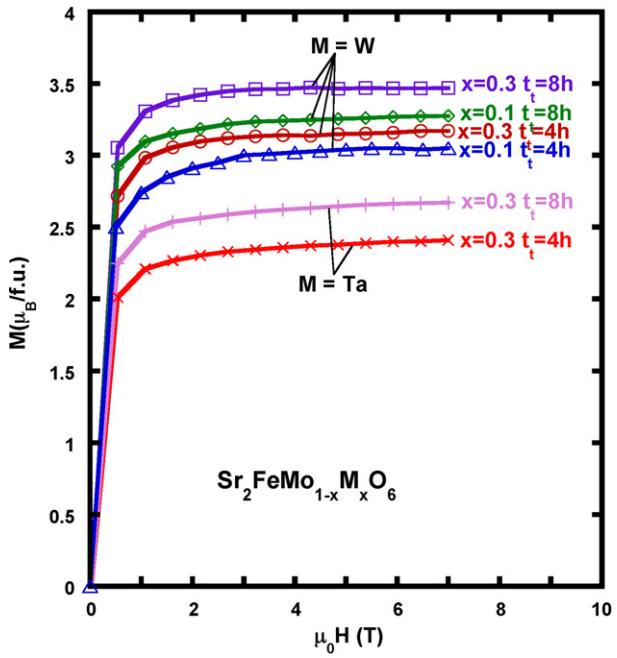

Fig. 4. Magnetization isotherms, at 4.2 K, for $Sr_2FeMo_{1-x}M_xO_6$ M = W (x = 0.1 and 0.3) and Ta (x = 0.3) sintered during 4 and 8 h, respectively.

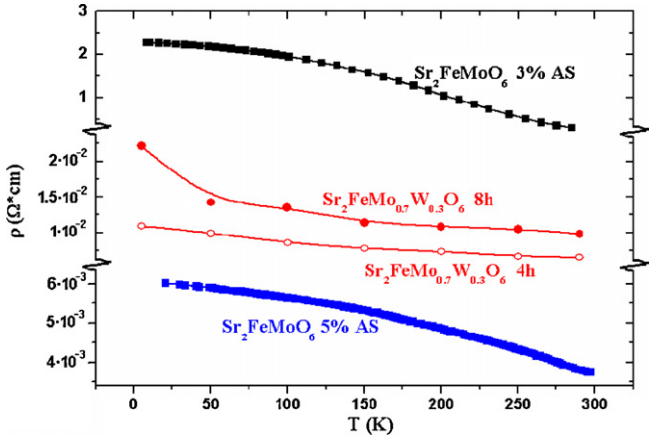

Fig. 5. Temperature dependences of the resistivities for $Sr_2FeMo_{0.7}W_{0.3}O_6$ perovskites, sintered 4 and 8 h, respectively. The resistivities of end series perovskites having 3% and 5% antisite defects are also shown [10].

the determined compositions are not greater than 1%. The compositions of the grains along a "line scan" was also analysed. A more uniform distribution of constituting elements along the grains can be shown in samples sintered at 1300 °C, 8 h. There is a little increase in Fe, Mo or W content for samples heated 8 h, as compared to those sintered during 4 h.

3.2. Magnetic properties

The magnetization isotherms, obtained at 4.2 K, for some $Sr_2FeMo_{1-x}M_xO_6$ perovskites with M = W and Ta are plotted in Fig. 4. Typical curves for ferromagnetic ordering, generally are shown. In some samples, the magnetizations increase with field suggesting the presence of a small contribution, of spin-glass type, superposed on a ferromagnetic one, particularly for samples sintered during 4 h. The saturation, of the ferromagnetic component, seems to be obtained in field of 2 T.

As showed already [7], in the case of Sr_2FeMoO_6 having 3% antisites defects, the saturation magnetization is 3.5 μ_B/f.u. When the antisites concentration is of 5%, the saturation magnetization decreased at 3.3 μ_B/f.u. The above values are below the theoretical spin-only moment of ferrous ions. As mentioned in Section 1, the magnetic state is strongly dependent on the degree of order. In a disordered sample, antiferromagnetic correlations associated with Fe–O–Fe superexchange interactions have been evidenced [4]. Thus, according to the degree of crystallographic order, there can be complex magnetic interactions which influence considerably the saturation magnetizations.

A more complex situation than in the case of Sr_2FeMoO_6, is present in W and Ta doped samples. As seen from Fig. 4, when increasing the sintering time, at 1300 °C, from 4 h to 8 h, the saturation magnetizations of the $Sr_2FeMo_{0.9}W_{0.1}O_6$ and $Sr_2FeMo_{0.7}W_{0.3}O_6$ increase from 3.1 μ_B/f.u. to 3.52 μ_B/f.u. and from 3.06 μ_B/f.u. to 3.18 μ_B/f.u., respectively. The structural analyses, evidenced, for the x = 0.1 and x = 0.3 samples doped with W, a decrease by 3% and 2.3%, respectively of the number of antisites when increasing sintering time (Table 1). If the ordering mechanism is followed by a changes of the corresponding number of iron from antiferromagnetic to ferromagnetic ordering, due to the diminution of antisite content, an increase of the magnetization by ≅0.23 μ_B/f.u. is expected, close to the observed difference in magnetizations of the above samples.

Previously, has been reported an increase of magnetization when W content increases in the composition range $x \leq 0.4$ [17]. In the present study, the magnetizations for $x \leq 0.3$ are little smaller than the value previously reported in highly ordered Sr_2FeMoO_6. This behaviour can be correlated with a higher number of antisite defects than in end series compound. At the grain boundary, due to an imperfect crystallization, the distribution of the constituting elements could be somewhat different from that inside the grain, particularly for samples sintered 4 h at 1300 °C. The spin-glass contribution, suggested by magnetic measurements, can be connected with crystal defects and with relative higher iron content at grain boundaries, as compared to a random distribution.

The Curie temperatures, T_c, of $Sr_2FeMo_{1-x}W_xO_6$ solid solutions, sintered during 8 h, decrease from 420 K (x = 0) to 363 K (x = 0.1) and 342 K (x = 0.3). The T_c value of the x = 0.3 sample, sintered during 4 h, is somewhat higher, T_c = 374 K, than the Curie temperature of the one sintered longer time. This may be connected with possible non-random arrangement of Fe atoms in some region of grains. This fact is also suggested by electron microscope studies, as already mentioned.

The saturation magnetizations of $Sr_2FeMo_{0.7}Ta_{0.3}O_6$ samples increase only by ≅0.12 μ_B/f.u. when sintering time increases. The relative small increase can be correlated with the little decrease of the number of antisites (≅1%), when the sintering time changes from 4 h to 8 h. For a similar composition, the decrease of the magnetization in Ta substituted samples, as compared to Sr_2FeMoO_6, is higher than that of W doped one. The Ta^{5+} seems to disrupt the double exchange interaction, responsible for the magnetism in Sr_2FeMoO_6, more efficiently than W^{6+}, as already suggested [27].

3.3. Resistive behaviour

The temperature dependences for resistivities of the $Sr_2FeMo_{0.7}W_{0.3}O_6$ samples, sintered at 1300 °C during 4 and 8 h, respectively are plotted in Fig. 5. On the same figure are given the resistivities of two Sr_2FeMoO_6 samples having 3% and 5% antisites, respectively, but differently elaborated [10]. A great difference between the resistivities of the two Sr_2FeMoO_6 samples is shown. In all cases the resistivities decrease with temperature. According to Niebieskikwiat et al. [30], the differences in the resistivities are due to different degree of grain boundaries (GB)

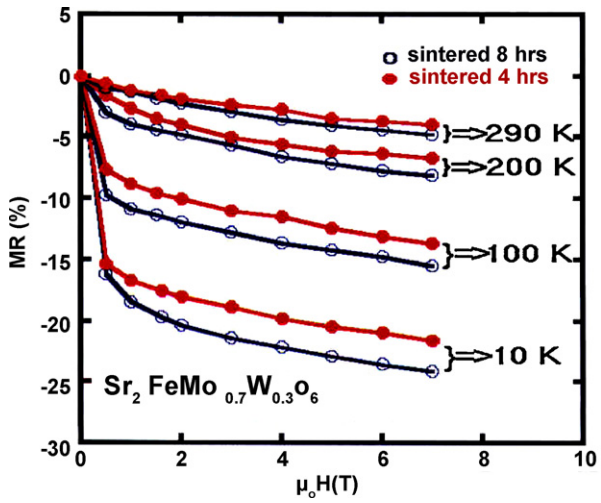

Fig. 6. Field and temperature dependences of the $Sr_2FeMo_{0.7}W_{0.3}O_6$ magnetoresistivities. The data obtained for sample sintered at 4 and 8 h are given.

oxidation. As the oxidation level increases, the GB resistance of the sample also does and the transport properties become dominated by the GB insulating barriers. In this situation, the electrical transport behaviour changes from metallic to insulating. In the case of pure Sr_2FeMoO_6 samples, the high resistivity has been obtained by heating in argon with 0.8% hydrogen (3% AS), while the other one having smaller resistivity in argon having 1.7% hydrogen (5% AS) [10] (Fig. 5). The grain boundaries oxidation, due to possible presence of oxygen impurities, was more effective in sample heated in argon with smaller hydrogen content.

The resistivities of $Sr_2FeMo_{0.7}W_{0.3}O_6$ sintered at 1300 °C, during 8 h are higher that those of the sample sintered 4 h. By keeping longer time at high temperature the degree of grain-boundary oxidation is expected to be increased since of possible oxygen impurities in argon. The resistivities are influenced also by the grain-boundary densities and hence by the grain dimensions, as well as their forms. Since resistivities depend also on annealing conditions, as temperature, atmosphere, etc., it is difficult to quantify (distinctly) the effect of the grain-boundary densities on transport properties.

The field and temperature dependences of the magnetoresistivities (MR) have been analysed. Higher absolute MR values can be seen in sample sintered during 8 h (Fig. 6). The contribution of magnetic state at the grain boundaries, in the intergrain tunnelling magnetoresistance (ITMR) of polycrystalline perovskites has been analysed [30,31]. Quantitative models to explain the ITMR are in principle the same as those proposed to explain the tunnelling MR in granular materials [31]. The polycrystalline sample can be described as a network of tunnel junctions whose electrodes are ideal double perovskite grains and an insulating oxide layer separating each one [32]. In the case of elastic tunnelling, across a single barrier and averaged over random grain orientations, the magnetoresistivities can be written as [31]:

$$\frac{\Delta\rho}{\rho_0} = -P^2 m(H)^2 [1 + P^2 m(H)^2]^{-1} \quad (1)$$

where P is the degree of spin polarization and $m(H)$ is the bulk magnetization, normalized to its saturation value.

The contribution of spin disorder to magnetoresistivity has been also considered [31]. This can be taken into account by adding a linear term, $-bH$, to the direct tunnelling model:

$$\frac{\Delta\rho}{\rho_0} = -P^2 m(H)^2 [1 + P^2 m(H)^2]^{-1} - bH \quad (2)$$

where H is external field and b a parameter not field dependent.

In the above model, it was assumed that the region near the grain boundaries is well ordered, with a polarization characteristic of the bulk material. This assumption is not true for a polycrystalline sample. According to Serrate et al. [31], the field dependence of the magnetoresistivities can be better described when the bulk magnetization, $m(H)$ is replaced by the magnetization from the disordered region near the grain boundaries, $m_g(H)$. Thus, the relation (2) is modified to:

$$\frac{\Delta\rho}{\rho_0} = -P^2 m_g(H)^2 [1 + P^2 m_g(H)^2]^{-1} - bH \quad (3)$$

As above, the term $-bH$ has been introduced to take into account the intragrain contribution to magnetoresistance. Assuming a spin-

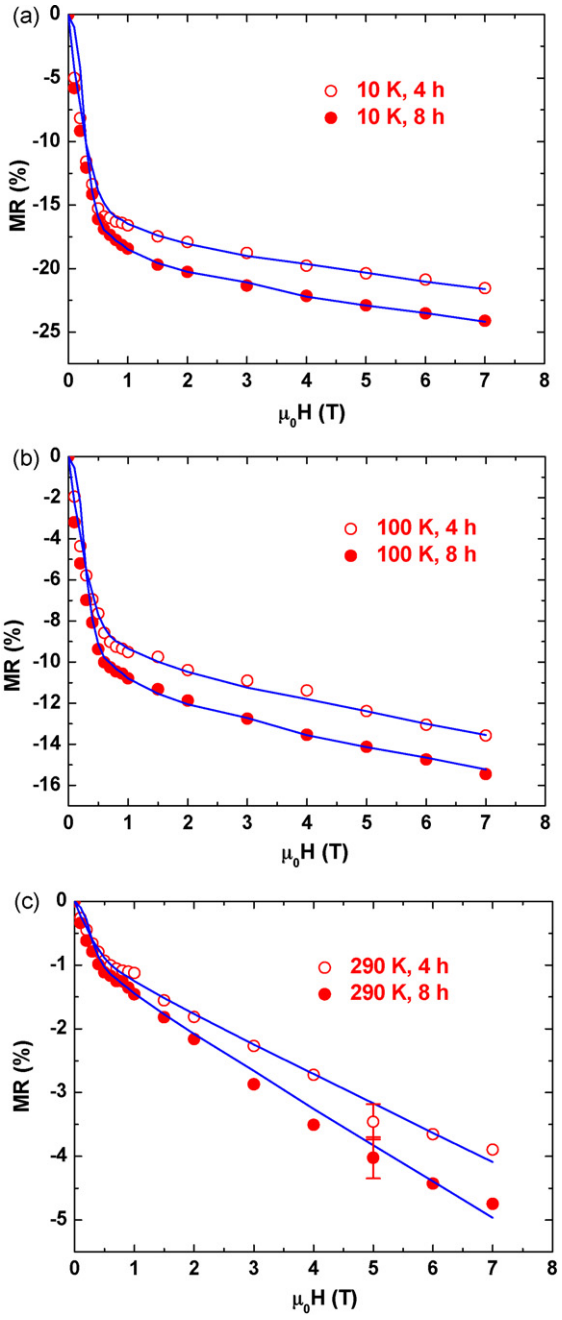

Fig. 7. The field dependences of the magnetoresistivities for $Sr_2FeMo_{0.7}W_{0.3}O_6$ at 10 K (a), 100 K (b) and 290 K (c). The data are for samples sintered at 1300 °C during 4 h (open circles) and 8 h (full circles). By solid lines are plotted the predictions of relation (2) with parameters P and b given in Fig. 8.

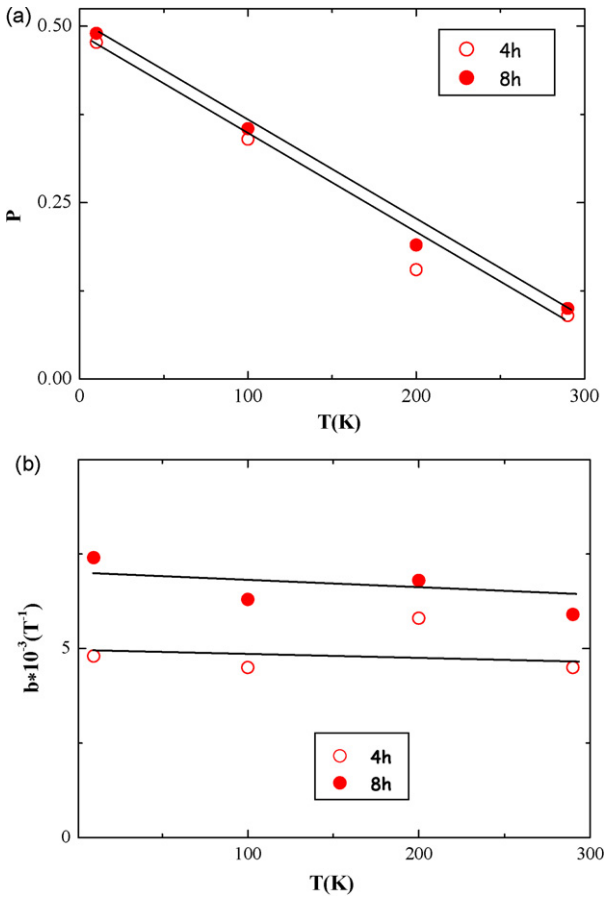

Fig. 8. Temperature dependences of polarizations, P (a) and of b values (b) in $Sr_2FeMo_{0.7}W_{0.3}O_6$ sintered during 4 h and 8 h, respectively.

glass model, with weak anisotropy field, the $m_g(H)$ behaviour can been described by the relation:

$$m_g(H) = (1 - aH^{-1/2}) \quad (4)$$

The above type of analysis has been used to describe the field dependences of the magnetoresistivities in (Ba,Sr)$FeMoO_6$ perovskites [31,33].

The field and temperature dependences of the magnetoresistivities in $Sr_2FeMo_{0.7}W_{0.3}O_6$ perovskites sintered, at 1300 °C, during 4 h and 8 h, respectively were analysed according to above models. It can be concluded that the relation (1) cannot describe the experimental results since of rather high intragrain contribution to magnetoresistivity, which is not considered in the model.

The field dependences of the magnetoresistivities, at some temperatures, as well as the prediction of relation (2), plotted as solid lines, are given in Fig. 7. The parameters P and b, obtained by fitting the experimental data are given in Fig. 8. In limit of experimental errors a rather good description of experimental evidence is shown. At 10 K, the polarization is around $P \cong 0.48$, slightly higher in samples sintered longer time. The b values seem to be not dependent on temperature and are higher for samples sintered during 8 h.

The magnetoresistivities of $Sr_2FeMo_{0.7}W_{0.3}O_6$ samples fitted with the relation (3) are shown in Fig. 9. A good description of experimental data, by the fitted curves with the parameters P, a and b, plotted in Fig. 10, is shown. The polarization determined at 10 K, is higher than predicted by fitting with relation (2). The polarizations are also higher in samples longer time thermally treated. The parameter a describing the approach to saturation law, from

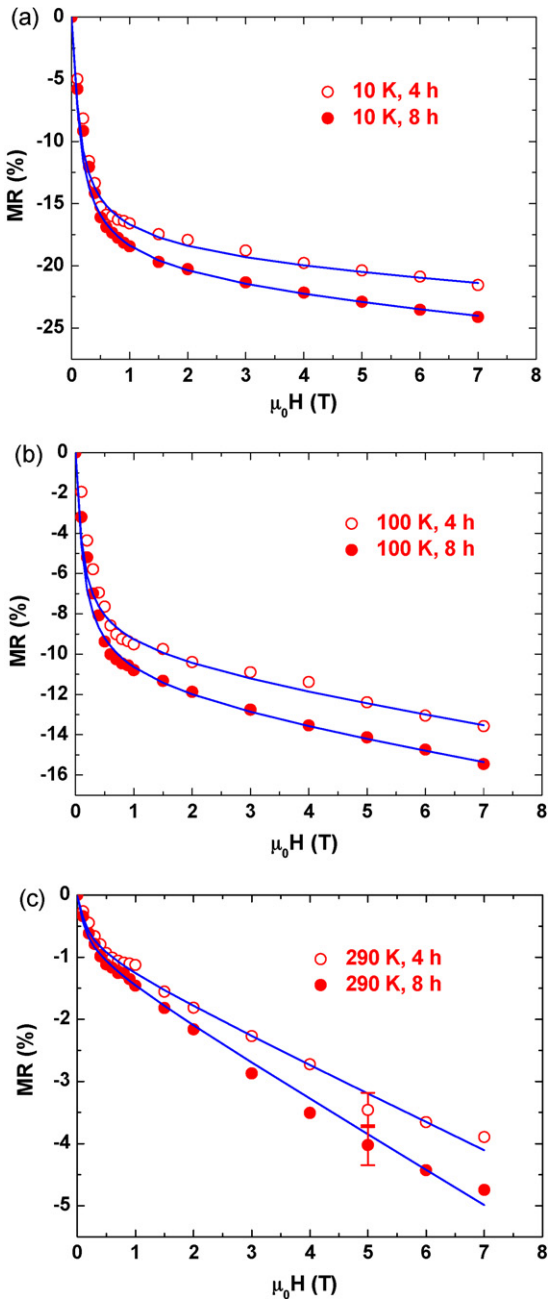

Fig. 9. The field dependences of the magnetoresistivities for $Sr_2FeMo_{0.7}W_{0.3}O_6$ at 10 K (a), 100 K (b) and 290 K (c). The data for samples heated during 4 h (open circles) those sintered at 1300 °C during 8 h (full circles) are given. By solid lines are plotted the predictions of relation (3) with the parameters given in Fig. 10.

relation (4), seems to be not temperature dependent. The value $a \cong 0.16\,T^{1/2}$ (where by T is denoted Tesla) is somewhat smaller than the reported one in ($Ba_{0.8}Sr_{0.2}$)$FeMoO_6$ sample, at low temperatures, but coincides with that determined at 250 K [31]. The b parameters, which describe the evolution of the magnetoresistivities inside the grain, increase with temperature, reflecting the tendency for spin disordering inside the grains.

As a conclusion, the relation (3) describes better the field and temperature dependences of the magnetoresistivities. The relation predicts, as expected, an increase of the spin disorder inside the grains, as temperature increased. A greater intragrain contribution to magnetoresistivities was also shown by increasing the sintering interval, as result of the diminution of the number of antisites. The prediction of the relation (2) concerning a spin disorder not

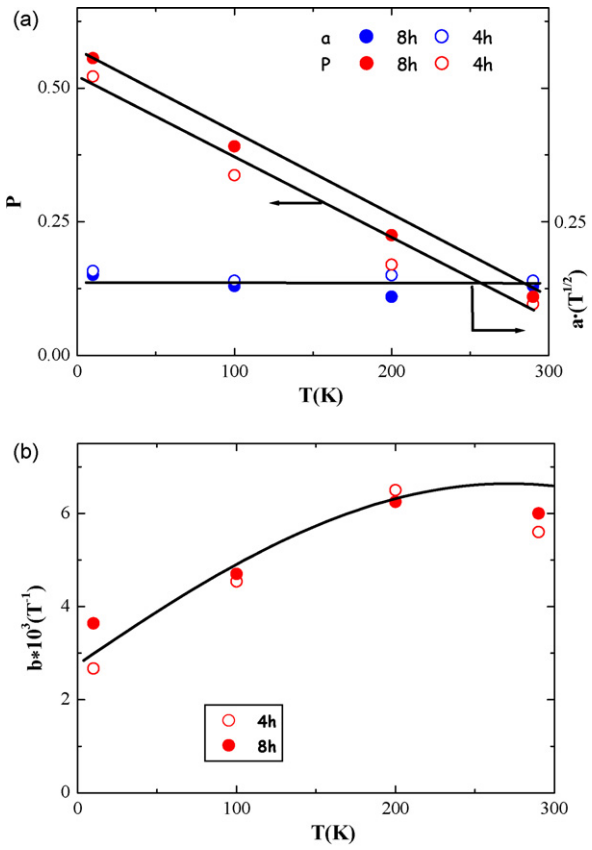

Fig. 10. Temperature dependences of the polarization, *P*, and a parameter obtained by fitting experimental data with relation (3) are shown in (a). In (b) is given the temperature dependence of the *b* values.

temperature dependent inside the grain has no physical reason (Fig. 8).

The determined polarizations, at 10 K, obtained by fitting the experimental data with the relation (3), are $P = 0.52$ and $P = 0.57$ for $Sr_2FeMo_{0.7}W_{0.3}O_6$ sintered 4 h (12.8% AS) and 8 h (10.5% AS), respectively. These values are very close to those experimentally determined and computed in Sr_2FeMoO_6 single crystal having 12.5% AS ($P = 0.53$). In Sr_2FeMoO_6 thin films, a polarization $P = 0.85$ has been reported [34]. A value $P = 0.25$ was determined in Sr_2FeMoO_6 having ≅12% AS, at 77 K [33], somewhat smaller than that obtained at this temperature in $Sr_2FeMo_{0.7}W_{0.3}O_6$ samples. Hemery et al. [33], stated that this value can be correlated with lower polarization in the intergrain region close to the grain boundaries, a wider intergrain insulating region as well as spin-flip scattering from defect states in the intergrain region. This matter has been further analysed on the basis of the magnetization and magnetoresistance studies on Sr_2FeMoO_6 and the independent control of the antisites defects and grain-boundary densities [35]. It has been proposed that MR is dominantly controlled by a mechanism derived from the magnetic polarization of grain-boundary regions acting like spin valves. According to our data, in agreement with the above proposals, it seems that the polarization is influenced both by the number of AS as well as on the grain-boundary regions.

We note that the relation (3) is valid when the applied magnetic field is smaller than the exchange field [31]. This requirement is satisfied in the present case. The range of external field, used in determining the magnetoresistivities, is not sufficient to saturate the contribution of the magnetization due to presence of a small spin-glass-type contribution superposed on the ferromagnetic one.

4. Conclusions

Two series of pseudo-quaternary double perovskites $Sr_2FeMo_{1-x}M_xO_6$ with M = W and Ta, were obtained by sintering at 1300 °C during 4 h and 8 h, respectively. The dimensions of the grains increased for samples sintered longer time. The EDS measurements evidenced, for the same sample, differences in the grain compositions. These differences decreased by increasing sintering time. As a result, narrower XRD lines can be shown. The number of antisite defects diminishes for samples sintered longer time. This is followed by an increase of magnetization as result of the diminution of the number of iron ions involved in antiferromagnetic superexchange interactions. The spin-glass contributions to magnetic ordering also decreased.

The magnetoresistivities of $Sr_2FeMo_{0.7}W_{0.3}O_6$ samples sintered 8 h are higher than of those sintered during 4 h. The experimental data were analysed by considering both the contributions of the intergrain tunnelling magnetoresistance (ITMR) as well as of spin disorder inside the grains. The ITMR contribution is particularly important in low external field region, commonly below 1.5–2 T, and temperatures $T < 200$ K. An intragrain contribution to magnetoresistivity is also present in the studied temperature range. This can be correlated with the presence of antisites defects enhanced by the presence of W. The diminution of the number of antisites, as result of increasing sintering time, leads also to an increased contribution to magnetoresistivity.

The polarizations obtained from experimental data are higher in samples treated longer time, having at 10 K, a value $P \cong 0.57$, for $Sr_2FeMo_{0.7}W_{0.3}O_6$. The polarizations seem to be influenced both by the number of AS, as well as the grain-boundary regions.

References

[1] P. Woodward, R.D. Hoffmann, A.W. Sleight, J. Mater. Res. 9 (1994) 2118.
[2] K.I. Kobayashi, T. Kimura, H. Sawada, K. Terakura, Y. Tokura, Nature 395 (1998) 677.
[3] R.P. Panguluri, S. Xu, Y. Moritomo, V. Solovyev, B. Nadgorny, Appl. Phys. Lett. 94 (2009) 012501.
[4] D. Sanchez, J.A. Alonso, M. Garcia-Hernandez, M.J. Martinez-Lope, J.L. Martinez, A. Mellergard, Phys. Rev. B 65 (2002) 104426.
[5] B. Martinez, J. Navarro, L. Balcells, J. Fontcuberta, J. Phys.: Condens. Matter 12 (2000) 10515.
[6] B. Garcia-Landa, C. Ritter, M.R. Ibarra, J. Balsco, P.A. Algarabel, R. Mahendiran, J. Garcia, Solid State Commun. 110 (1999) 435.
[7] K. Kuepper, I. Balasz, H. Hesse, A. Winiarski, K.C. Prince, M. Matteucci, D. Wett, R. Szargan, E. Burzo, M. Neumann, Phys. Stat. Solidi (a) 201 (2004) 3252.
[8] J.S. Kang, J.H. Kim, A. Sekiyama, S. Kasai, S. Suga, S.W. Han, K.H. Kim, T. Muro, Y. Saitoh, C. Hwang, C.G. Olson, B.J. Park, B.W. Lee, J.H. Sim, J.H. Park, B.I. Min, Phys. Rev. B66 (2002) 113115.
[9] J. Linden, T. Yamamoto, M. Karppinen, H. Yamauchi, T. Pietari, Appl. Phys. Lett. 76 (2000) 2925.
[10] M. Raekers, K. Kuepper, H. Hesse, I. Balasz, I.G. Deac, S. Constantinescu, E. Burzo, M. Valeanu, M. Neumann, J. Opt. Adv. Mater. 8 (2006) 455.
[11] E. Burzo, I. Balasz, S. Constantinescu, I.G. Deac, J. Magn. Magn. Mater. 316 (2007) e741.
[12] M.S. Moreno, J.E. Gayone, M. Abbate, A. Caneiro, D. Niebieskikwiat, R.D. Sanchez, A. de Siervo, R. Landers, G. Zampieri, Solid State Commun. 120 (2001) 161.
[13] V. Kanchana, G. Vaitheeswaran, M. Alouani, A. Delin, Phys. Rev. B75 (2007) 220404.
[14] J. Navarro, C. Frontera, D. Rubi, N. Mestres, J. Frontcuberta, Mater. Res. Bull. 38 (2003) 1477.
[15] K. Kuepper, M. Raekers, C. Taubitz, H. Hesse, M. Neumann, A.T. Young, C. Piamonteze, F. Bondino, K.C. Prince, J. Appl. Phys. 104 (2008) 036103.
[16] E. Burzo, Landolt Bornstein Handbuch, vol. III-27f1β, Springer Verlag, 1996.
[17] K.I. Kobayashi, T. Okuda, Y. Tomioka, T. Kimura, Y. Tokura, J. Magn. Magn. Mater. 218 (2000) 17.
[18] R.I. Dass, J.B. Goodenough, Phys. Rev. B 63 (2001) 064417.
[19] N.E. Massa, J.A. Alonso, M.J. Martinez-Lope, M.T. Casais, Phys. Rev. B 72 (2005) 214303.
[20] R. Ward, J. Longo, J. Am. Chem. Soc. 83 (1961) 2816.
[21] F.K. Patterson, C.W. Moeller, R. Ward, Inorg. Chem. 2 (1963) 196.
[22] S. Ray, A. Kumar, S. Majumdar, E.V. Sampathkumaran, D.D. Sarma, J. Phys.: Condens. Matter 13 (2001) 607.
[23] F. Bardelli, C. Meneghini, S. Mobilio, S. Ray, D.D. Sarma, J. Phys. Condens. Matter 21 (2009) 195502.

[24] M. Karppinen, H. Yamauchi, Y. Yasukawa, J. Linden, T.S. Chan, R.S. Liu, J.M. Chen, Chem. Mater. 15 (2003) 4118.
[25] P.D. Battle, T.C. Gibb, A.J. Herod, S.H. Kim, P.H. Munns, J. Mater. Chem. 5 (1995) 865.
[26] E.J. Cussen, J.F. Vente, P.D. Battle, T.C. Gibb, J. Mater. Chem. 7 (1997) 459.
[27] J. Linden, T. Yamamoto, J. Nakamura, H. Yamauchi, M. Karppinen, Phys. Rev. B 66 (2002) 184408.
[28] DIFRAC plus TOPAS General profile and structure analysis software for powder diffractions data, USER's MANUAL, version 2.0, Bruker AXS Gmb, Karlsruhe, 2001.
[29] A.A. Cohelo, J. Appl. Cryst. 36 (2003) 86.
[30] D. Niebieskikwiat, F. Prado, A. Caneiro, R.D. Sanchez, Phys. Rev. B 70 (2004) 132412.
[31] D. Serrate, J.D. De Teresa, P.A. Algarabel, M.R. Ibarra, J. Gallibert, Phys. Rev. B 71 (2005) 104409.
[32] J. Inoue, S. Maekawa, Phys. Rev. B 53 (1996) R11927.
[33] E.K. Hemery, G.V.M. Williams, H.J. Trodahl, Physica B390 (2007) 175.
[34] M. Bibes, K. Bouzehouane, A. Barthelemy, M. Besse, S. Fusil, M. Bowen, P. Seneor, J. Carrey, V. Cros, A. Vaures, J.P. Contour, A. Fert, Appl. Phys. Lett. 83 (2003) 2629.
[35] D.D. Sarma, S. Ray, K. Tanaka, M. Kobayashi, A. Fujimori, P. Sanyal, H.R. Krishnamurthy, C. Dasgupta, Phys. Rev. Lett. 98 (2007) 157205.